

SCIENTIFIC REPORTS



OPEN

Ultrafast nonlinear optical response in solution dispersions of black phosphorus

Lili Miao^{1,2}, Bingxin Shi³, Jun Yi¹, Yaqin Jiang⁴, Chujun Zhao¹ & Shuangchun Wen¹

We report the spatial self-phase modulation (SSPM) effect for solution dispersions of black phosphorus (BP). The experimental results suggest that this concentration-dependent coherent light diffraction is due to the ultrafast and large third-order optical nonlinearity of BP. The third-order nonlinear susceptibility of BP has been simply obtained about $10^{-19} \text{ m}^2/\text{V}^2$ by analyzing the experimental results. The fast relaxation time during dynamic relaxation is obtained as 0.13 ps. Our experimental results imply novel potential application of BP in ultrafast nonlinear phase modulation devices based on their nonlinear optical response.

Low dimensional optical materials with ultrafast response and strong nonlinearity have exhibited novel physics and tremendous application potential in optical communication, optical sensing, medical diagnosis, etc¹⁻⁶. Inspired by the emergence of two-dimensional atomic crystal graphene, the nonlinear optics of graphene and graphene-like materials have been explored intensively in recent years endowed for their excellent nonlinear response and broadband applications⁷⁻¹⁰. Besides graphene, black phosphorus (BP), a newly rising graphene-like material with natural band gap, has shown tremendous and intriguing physical, chemical, and electronic properties¹¹⁻¹³. The BP has a thickness dependent direct band gap that changes from 0.3 eV in the bulk to 1.88 eV in a monolayer¹⁴. It can also be switched between insulating and conducting states, and it is still flat enough to confine electrons so that charge flows quickly, comparable with those in single layer of molybdenum disulphide¹⁵. Sample mobility is also found to be thickness dependent, with the highest value up to $\sim 1000 \text{ cm}^2/\text{Vs}$ obtained at thickness $\sim 10 \text{ nm}$ ¹⁶. Furthermore, the BP photodetector shows time response of 1 ms (rise) and 4 ms (fall), making few-layer BP a promising active 2D material in broadband and fast photodetectors across the visible and near infrared region¹⁷. In addition, BP is made from a single element, in theory, the pure samples are easier to obtain. Compared to other graphene-like 2D materials, tunable optical properties and direct bandgap for all thicknesses of BP may bring significant benefits to a variety of fascinating photonics applications.

Besides its high electron mobility, BP has unique optical properties, such as the strong in-plane anisotropic¹⁸. Considering the tunable band-gap, the electronic and optical performance of the materials can change dramatically consequently. Beyond the linear optics regime, the optical properties, especially the ultrafast optical response and the nonlinear optical properties of BP in case of different thicknesses, various doping conditions, and different polarization directions of the excitation light, have been paid more attention recently. The ultrafast relaxation dynamics of BP have been investigated by the pump-probe technique¹⁹⁻²¹, and the fast recovery time in BP was determined to be $\sim 24 \text{ fs}$ at 1550 nm ²⁰, 16 and 32 fs for 800 and 2026 nm pulses²¹, which is much faster than that of previous 2D crystal materials, such as graphene ($\sim 1.27 \text{ ps}$)²² and MoS_2 ($\sim 2.1 \text{ ps}$)²³. R. Suess *et al.* reported the anisotropic carrier dynamic with faster time to be $\sim 180 \text{ ps}$ at 780 nm in BP, which may be induced by hot carriers cooling¹⁹. In another aspect, the third-order nonlinear optical responses of BP have been investigated and characterized via Z-scan technique, third-harmonic generation (THG) method, etc²⁴⁻²⁶. The open-aperture (OA) Z-scan experiments demonstrate that BP has perfect saturable absorption performance at both optical communication band (1550 nm) and visible band (532 nm and 680 nm), making BP a preferred alternative material for saturable absorbers (SAs)²⁰. The broadband nonlinear optics response of few-layer BP towards mid-infrared has also been reported by S. Lu *et al.*²⁴. In addition, X. Zheng *et al.* reported a transition from saturable absorption (SA) to reverse saturable absorption (RSA) with the increase of laser intensity²⁶. Moreover, both the passive Q-switching

¹Key Laboratory for Micro-/Nano- Optoelectronic Devices of Ministry of Education, School of Physics and Electronics, Hunan University, Changsha, 410082, China. ²Femtosecond Optics Group, Department of Physics, Imperial College London, London, SW7 2BW, UK. ³Wuhan Optics Valley Aerospace Sanjiang Laser Industrial Technology Research Institute Co. Ltd., Wuhan, 430000, China. ⁴Troop NO. 95829, Xiaogan, 432100, China. Correspondence and requests for materials should be addressed to C.Z. (email: chujunzhao@gmail.com)

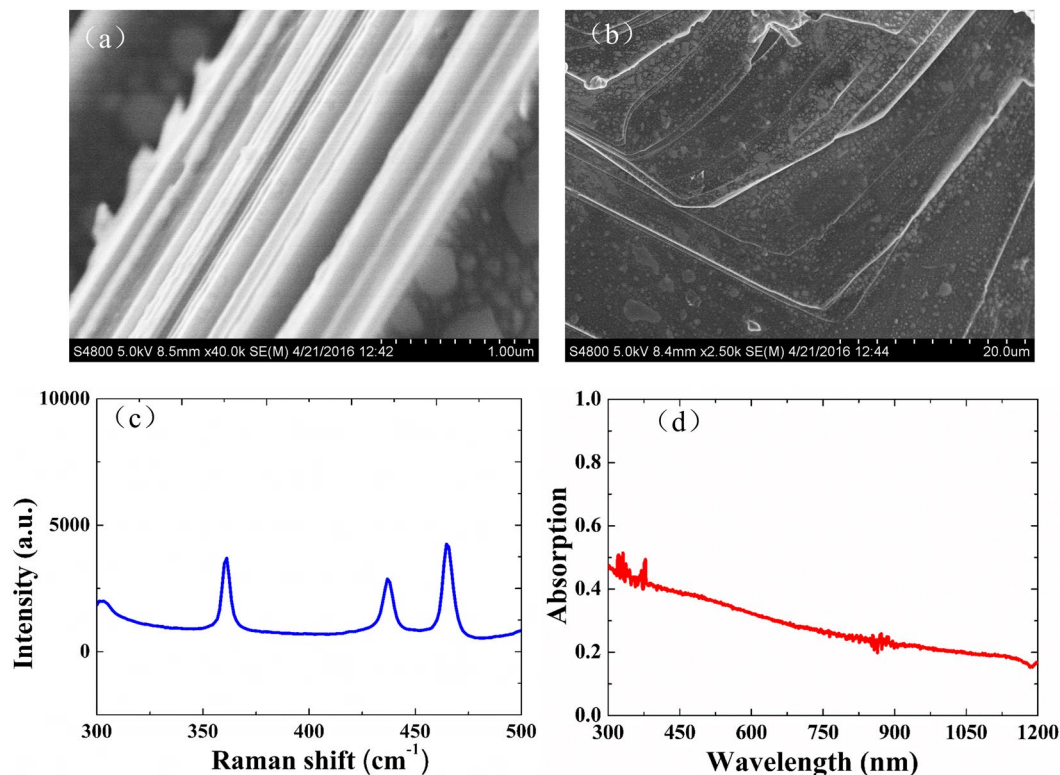


Figure 1. (a) and (b) SEM image of BP crystal, the scale bars are 1 μm (a) and 20 μm (b), respectively; (c) Raman spectra of BP; (d) Absorption spectrum of BP dispersion solutions in ethylene glycol.

and the mode-locking operation of the erbium-doped fiber lasers with the BP-SA have been experimentally demonstrated²⁷. D. Li *et al.* studied the thickness and polarization dependent linear and nonlinear optical properties of BP thin films, and then utilized their nonlinear absorption property to generate ultrafast and large-energy pulse with BP integrated fiber devices²⁸.

Besides Z-scan and THG methods, spatial self-phase modulation (SSPM), a phenomenon that the intensity dependence of the refractive index in nonlinear optical media occurs, is a manifestation of the coherent response of the material. SSPM was originally observed in liquid-crystal^{29, 30}, then later in nanomaterials, such as carbon nanotubes (CNTs) solutions³¹, graphene³², graphene oxide³³, topological insulators³⁴, transition metal dichalcogenides (TMDs)^{35, 36} and many other materials. While this manuscript was in preparation, a relevant work was published³⁷. It reports the broadband spatial self-phase modulation of BP, and the nonlinear refractive index of BP (~ 5 layers) is measured to be $\sim 10^{-9} \text{ m}^2/\text{W}$ and the third order nonlinear susceptibility is $\chi^{(3)} \sim 10^{-8} \text{ esu}$ at multiple wavelengths (equals $\chi^{(3)}$ to be $10^{-16} \text{ m}^2/\text{V}^2$)³⁷. Youngblood *et al.* report the $\chi^{(3)}$ of multilayer (~ 29 layers) BP to be $10^{-19} \text{ m}^2/\text{V}^2$ via layer tunable THG²⁵, while Zheng *et al.* reported a nonlinear refractive index value of $\sim 10^{-13} \text{ m}^2/\text{W}$ (~ 50 – 100 layers) at 800 nm femtosecond pulsed Z-Scan measurement²⁶. In addition, from other perspective, these methods have given the different nonlinear optical parameters of BP^{25, 26, 37}. It is exactly these disagreements that create the need for additional experimental and theoretical investigations to fully characterize the nonlinear susceptibility of BP further. In this work, we studied the phenomenon of SSPM for solution dispersions of BP under different concentration and laser intensity. The ultrafast nonlinear optical response was unambiguously observed and this coherent light diffraction is due to the remarkably large third-order nonlinearity. The third-order nonlinear refractive index of BP was then simply and exactly obtained by analyzing the experimental results.

Results

Characterizations of black phosphorus. Uniform few-layer BP dispersions have been prepared by the liquid phase exfoliation (LPE) method, which is a simple and effective technique to prepare two dimensional (2D) materials from layered bulk crystals towards multiple layered structures. Figure 1 shows the characterization of the BP sample. The scanning electron microscopy (SEM) image of BP crystal is shown in Fig. 1a,b, from which the high quality and flat layered surface of BPs can be verified from both lateral (a) and top (b) view, respectively. As shown in Fig. 1c, there are three Raman peaks at 361.15 cm^{-1} , 436.85 cm^{-1} , and 464.68 cm^{-1} from the multi-layer phosphorus corresponding to the A_g^1 , B_{2g} , and A_g^2 modes, respectively. Figure 1d shows the linear absorption spectrum of the BP solution dispersions in ethylene glycol ranging from 300 to 1200 nm, measured by the spectrometer (Perkins Elmer Lambda750). The profile is nearly flat with a smooth absorption curve in the ultraviolet up to near-infrared (UV-NIR) wavelength band, suggesting that multi-layer BP dispersions might be a promising broadband optical material.

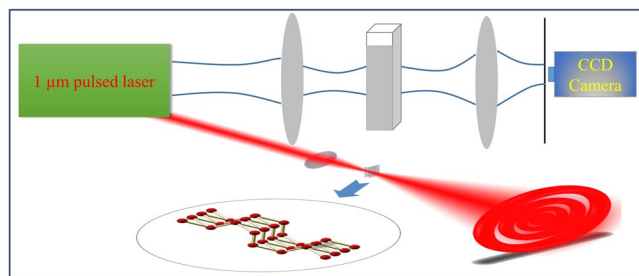


Figure 2. Experimental schematic diagram for SSPM experiment.

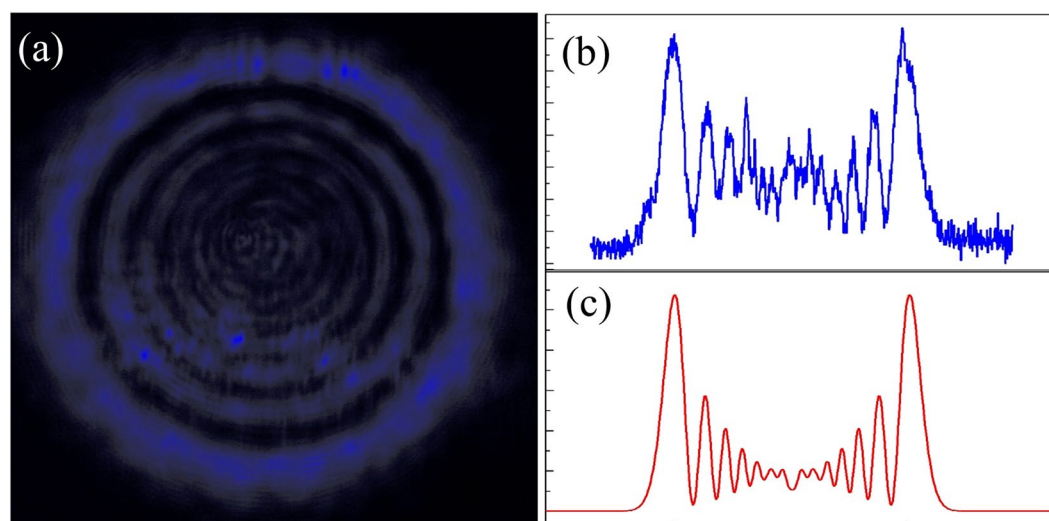


Figure 3. (a) The diffraction rings irradiated by 1061 nm ultrafast laser; (b) The axial intensity distribution of (a); and (c) The corresponding simulated intensity distribution.

Ultra-fast SSPM response. Inspired by the unique electronic and optical properties of BP, we have experimentally observed the SSPM phenomenon of BP. In the experiment, the ultrafast pulse laser was used to characterize the SSPM effects of BP solution dispersions. The linearly polarized beam from a 1061 nm (repetition rate of 2.7 MHz and pulse duration of 220 ps) laser was firstly focused by a lens of focal length 150 mm, causing high intensity illumination to the sample. A quartz cuvette of 5 mm thickness was used to contain the BP solution dispersions and placed before the beam focus. The distance between the focus and the front surface of the cuvette was 20 mm. Then the transmitted spectrum was collected by a CCD camera (Coherent LaserCam HR), which is 200 mm away from the focal lens. The schematic diagram was shown in Fig. 2.

Owing to the nonlinear index change induced by the nonuniform Gaussian profile of the light beam, we observed obvious diffraction ring pattern in the far field. Figure 3a is a typical pattern of diffraction rings caused by spatial self-phase modulation when the sample was irradiated by 1061 nm ultrafast laser. Figure 3b is the corresponding intensity distribution of the experimental result, and Fig. 3c illustrates the corresponding far field intensity distribution simulated by means of the Fraunhofer approximation of the Fresnel–Kirchhoff diffraction formula. From the figure, we conclude that the experimental result is in a good agreement with the theoretical one. Measurements of the pure ethylene glycol did not show a nonlinear response for the intensity ranges that were investigated here and, therefore, confirm that the observed nonlinear behavior is from the presence of the BP (*see supporting information*).

To confirm the presence of the BP induces the nonlinear refractive index in the medium and causes the SSPM effect in laser beam propagation, we performed concentration-dependence measurements. Figure 4a,b show the typical development of diffraction rings of SSPM when the input average power is 100 mW. They both emerged from the center of the patterns with all their diameters enlarging gradually and they deformed with irradiation time evolution and finally become stable during one second. As shown in Fig. 4a, it takes about 0.95 second for the development of diffraction rings, which includes emerging, enlarging and deforming. While varying the concentration of the BP solution dispersion, the number of diffraction pattern increases, and the nonlinear response will become much faster with higher BP concentration. As the SSPM phenomena are proportional to the absorption of the nonlinear medium, pattern formation time, the size and number of rings become larger with the increasing of the concentration. Figure 4c shows the final stable patterns for four different concentrations of solution dispersions under the same input average power 140 mW, where the concentration decreases gradually from 15 vol.% to 7.5 vol.%, respectively. We can observe that both numbers and diameters of the diffraction rings decrease with the

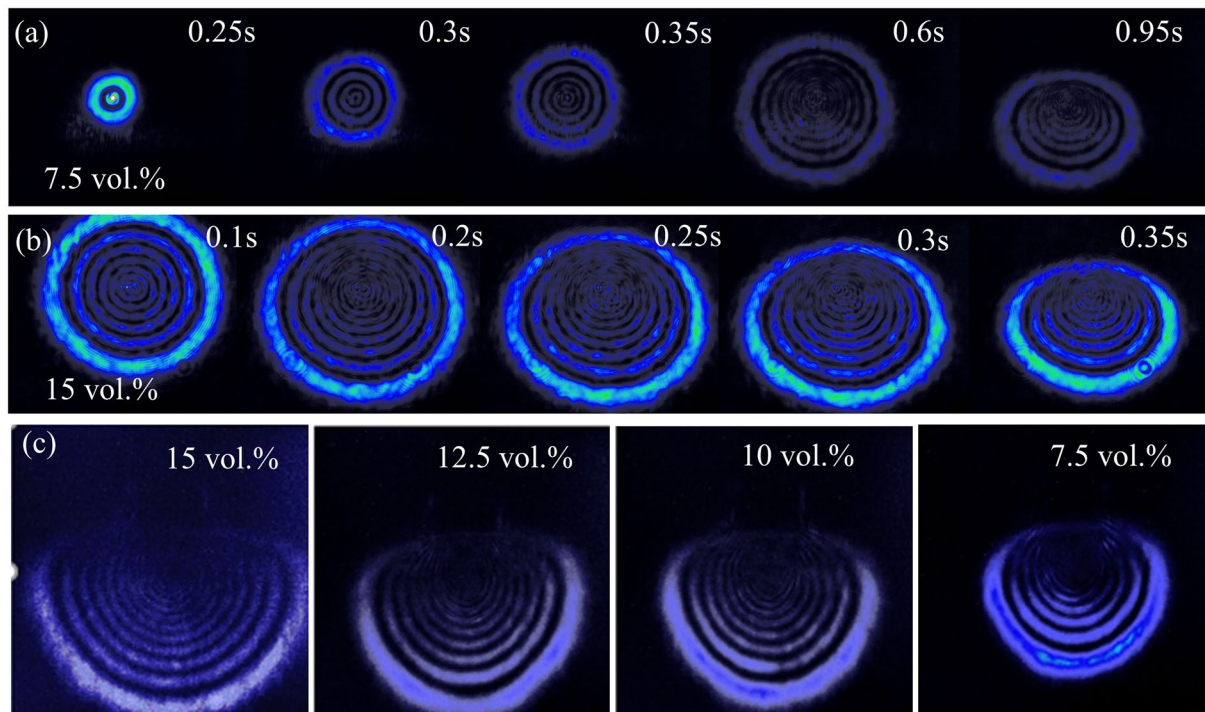


Figure 4. Snapshots of the pattern formation of: (a) Diluent BP solution dispersions (~7.5 vol.%); (b) 15 vol.% dispersion under the irradiance of 100 mW and (c) Different concentration under the irradiance of 140 mW at 1061 nm laser beam excitations.

concentration. These results verify that diffraction rings are mainly derived from the nonlinear optical properties of BP.

We also performed intensity-dependence measurements with the same experimental setup to convince the nonlinear response of the BP dispersion. The input laser power increases gradually from Fig. 5a–f as 60, 80, 100, 110, 130 and 140 mW, respectively. It can be observed that by increasing the laser power, the number of rings and the vertical asymmetry of the diffraction ring patterns increased. Consequently, one can evidently confirm that when the input laser power becomes higher, the propagating beam suffers more serious distortions.

The refractive index of many materials can be described by the relation

$$n = n_0 + n_2 I \quad (1)$$

where n_0 is the linear refractive index and I is the laser intensity and n_2 is the coefficient of the intensity-dependent refractive index³⁸. The total refractive index increases with increasing optical intensity. A corresponding phase shift $\Delta\psi$ of the beam traversing the nonlinear medium³²:

$$\Delta\varphi(r) = \frac{2\pi n_0}{\lambda} \int_0^{L_{\text{eff}}} n_2 I(r, z) dz \quad (2)$$

where r is the radial coordinate of the beam, λ is the wavelength of incident laser, L_{eff} is the total propagation length contributing to the SSPM.

We assume, for simplicity, that

$$\Delta\varphi(r) = \Delta\varphi(0) \exp\left(\frac{-2r^2}{\omega^2}\right) \quad (3)$$

where ω is the beam radius, as a constant. When $r \in [0, +\infty)$, there is r_1 and r_2 possessing the same wave vector and can interfere, which can be expressed as²⁹:

$$\frac{d\Delta\varphi(r_1)}{dr} = \frac{d\Delta\varphi(r_2)}{dr} \quad (4)$$

The constructive or destructive interference occurs and results appearance of diffraction rings.

$$\Delta\varphi(r_1) - \Delta\varphi(r_2) = m\pi \quad (5)$$

where m is an even or odd integer. The number of diffraction rings appeared can be estimated as²⁹:

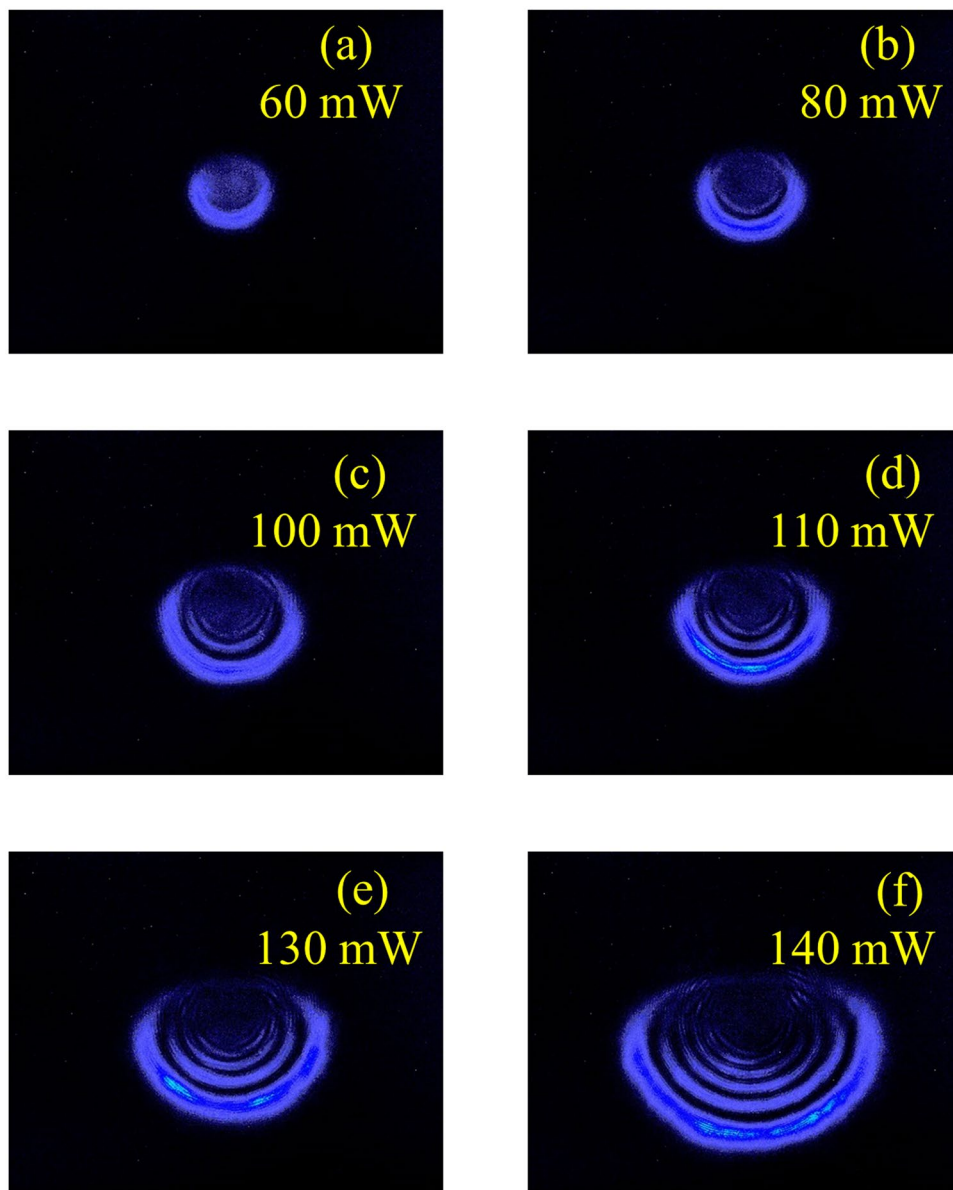


Figure 5. BP solution dispersions (~7.5 Vol.%) under input laser power increasing gradually from (a) to (f) as (a) 60, (b) 80, (c) 100 (d) 110, (e) 130 and (f) 140 mW, respectively.

$$N = \frac{\Delta\varphi(0) - \Delta\varphi(r)}{2\pi} \quad (6)$$

Assuming $\Delta\psi(r) = 0$, thus, $N = \Delta\varphi_0/2\pi$, we can obtain the equation to solve n_2 ³²:

$$n_2 = \left(\frac{\lambda}{2n_0 L_{eff}} \right) \frac{N}{I} \quad (7)$$

The nonlinear refractive index and the third-order nonlinear susceptibility of BP at different concentrations have been summarized in Table 1. We compared the rings number, and nonlinear refractive index n_2 at different concentration and input power which corresponds to different input intensity. At lower concentration, n_2 increases with input power or intensity, while the saturation of n_2 occurs due to sample concentration increase, as shown in Fig. 6. In our experiment, N is approximately proportional to I and the total refractive indexes increase with increasing optical intensity. The threshold for observing diffraction rings is about $0.58 \times 10^5 \text{ W/cm}^2$ for 15 vol.% and $0.97 \times 10^5 \text{ W/cm}^2$ for 7.5 vol.% BP solution dispersions. The nonlinearity n_2 can be easily obtained by finding N/I at the maximum laser power. We can estimate n_2 as $4.35 \times 10^{-12} \text{ m}^2/\text{W}$ for 15 vol.% and $1.45 \times 10^{-12} \text{ m}^2/\text{W}$ for 7.5 vol.% BP solution dispersions. The third order nonlinear susceptibility of BP was calculated to be $10^{-14} \text{ m}^2/\text{V}^2$

Volume fraction (vol.%)	$N_{\text{ring number}}$	n_2 ($10^{-12} \text{ m}^2/\text{W}$)	$\chi_{\text{total}}^{(3)}$ ($10^{-14} \text{ m}^2/\text{V}^2$)	$N_{\text{layer number}}$	$\chi_{\text{single layer}}^{(3)}$ ($10^{-19} \text{ m}^2/\text{V}^2$)
15	6	4.35	3.32	590	0.92
12.5	5	3.63	2.77	480	1.2
10	3	2.17	1.65	400	1.03
7.5	2	1.45	1.11	340	0.96

Table 1. The sample concentration and nonlinear optical parameters.

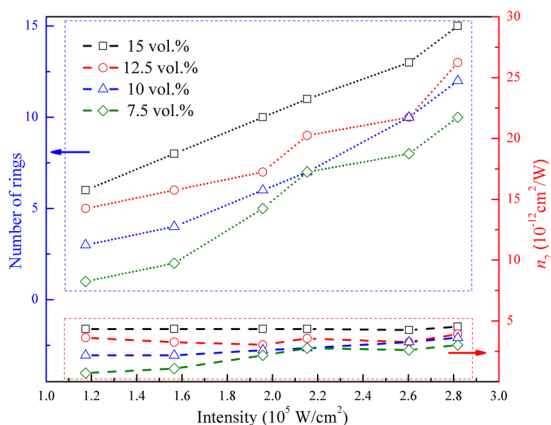


Figure 6. Relation between number of rings, nonlinear refractive index and input laser intensity.

(see supporting information). We use SI units here to avoid confusion. We estimate that $\chi_{\text{total}}^{(3)} = M^2 \chi_{\text{single layer}}^{(3)}$ ³². The number of effective layers M can be obtained as $M = \frac{C \times V \times N_A}{S/a^2}$, where V is the volume of the solution of 1.5 mL. The total number of (BP) molecules in the solution is $C \times V \times N_A$, where N_A is the Avogadro's number, S is the area of the cross-section of the cuvette ($= 1 \text{ cm} \times 3 \text{ cm}$), the total number of molecules in one effective layer is S/a^2 , where a ($\sim 4.5 \text{ \AA}$) is the lattice constant of BP³⁹. In our experiment, M is on the order of 300 to 600, thus the estimated $\chi_{\text{single layer}}^{(3)}$ is of the order of $10^{-19} \text{ m}^2/\text{V}^2$, which agrees with Z-scan measurements (~ 50 – 100 layers)²⁶, two orders of magnitude larger than estimated from THG experiments (~ 29 layers)²⁵, but more than two orders of magnitude smaller than that from ref. 37 (~ 5 layers). The variation of nonlinear susceptibility by different methods can be attributed to the difference of BP thickness, as BP possesses a thickness-dependent energy band gap. Further efforts, from both theoretical and experimental sides, are needed to fully understand the third-order nonlinear optical response of BP, e.g. the relationship between formation time and BP concentration. The measurement uncertainty comes from several aspects: the calculation of incident pulse laser intensity, the measurement of distance between lens, sample, CCD camera, the concentration and uniformity uncertainty of the BP sample during the formation of diffraction ring, and the counting of diffraction rings number, which is a key parameter in calculating the nonlinear coefficient for BP. However, by well-designed experimental scheme and data analysis, SSPM phenomena can be regarded as an effective method to estimate the orders of magnitude of the nonlinear refractive index.

Carrier dynamics. The ultrafast nonlinear response of BP was also investigated by time-resolved optical degenerate pump-probe transmission measurement. Femtosecond (fs) laser (Coherent Libra-S), which gave an output with a pulse repetition rate of 1 kHz, a central wavelength of 800 nm and a pulse duration around 100 fs, was employed in the time-resolved pump-probe experiment. The output laser beam was split into two different laser beams, one intense portion with a peak intensity of $75 \text{ GW}/\text{cm}^2$ as the pump beam to generate the photo-induced carriers, and the other weak portion with peak intensity of $0.3 \text{ GW}/\text{cm}^2$ as the probe beam. Figure 7 presents the carriers dynamic relaxation process for the BP suspension. The delay kinetics can be well fitted with a bi-exponential decay function:

$$\frac{\Delta T}{T} = A_1 e^{-t/\tau_1} + A_2 e^{-t/\tau_2} \quad (8)$$

where $\Delta T/T$ is defined as the relative change of the probe transmissivity caused by the pump, and τ_1 is the decay time with the respective amplitude weights A_1 . The fast and slow relaxation time is fitted to be 0.13 ps and 1.15 ps, respectively. We attribute the SSPM effect a transient phenomenon. The interaction and diffraction can occur under the well-defined phase difference between photons. To the ultrafast laser pulse, the carriers will relax in only about several pico-seconds, while every pulse is in the temporal slot of $0.37 \mu\text{s}$ (1061 nm, 2.7 MHz).

Therefore, the incident laser pulse is considered to be independent to each other, which confirms the transient effect of SSPM. The physical mechanism of the nonlinearity may be attributed to the reorientation and alignment of the BP nanosheets induced by the electromagnetic field, which is similar to the case of liquid crystals²⁹. Under

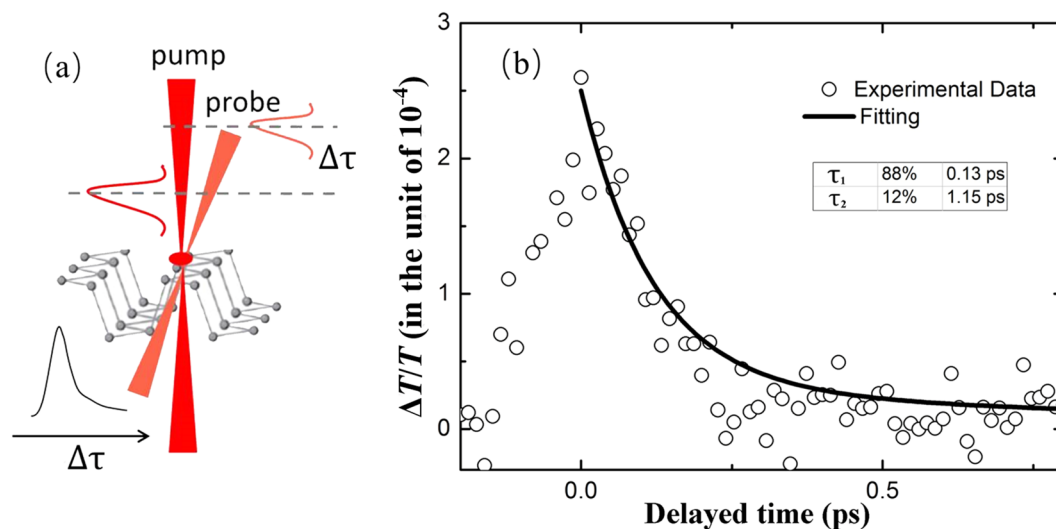


Figure 7. (a) Diagrammatic of carrier dynamics of BP solution; (b) Experimental results of pump-probe, scattered points are experimental results and solid lines are the fitting results.

the intense laser irradiation, the polarization state will relocate to a new array which is parallel to each other. The reoriented sheets can help light beam become coherent and form SSPM rings.

Conclusions

In conclusion, the third-order nonlinear susceptibility of BP dispersions was measured to be $10^{-19} \text{ m}^2/\text{V}^2$ and can be tuned via changing its concentration. Upon illumination, the BP solution dispersions show obvious SSPM response to the excitation wavelengths, demonstrating its ultrafast nonlinear response. Experimental results of BP under pulse illumination are fitted with a good correspondence between experimental and numerical results, which suggest that this coherent light scattering is due to the ultrafast, and large third-order optical nonlinearity of BP. The fast relaxation time during dynamic relaxation is obtained as 0.13 ps. Our experimental results exhibit the practical potential of this promising material for various nonlinear and ultrafast optoelectronics applications (e.g., ultrafast lasers, optical switches and modulators). Moreover, our work may provide an inroad for measuring key parameters, such as molecular weights of the solvent and the nanomaterials based on their novel nonlinear optical response. The technique can further be used to study the composition, purity and stability of other nanomaterials at broadband wavelength, including those with potential for clinical applications.

Methods

Materials. To begin, bulk BP crystal (purchased from Smart Elements) was grinded to BP powder. Then the powder was dispersed into ethylene glycol, along with ultra-sonicated for 2 hours. After sonication, the phosphorene in ethylene glycol was centrifuged at a speed of 15000 rpm for 20 minutes. The upper ~80% which contains few layers was decanted for analysis and the dispersions were settled for more than 20 hours to make sure that there is no large size sedimentations during our experiments. BP dispersions were then diluted to 4 samples (15 vol.%, 12.5 vol.%, 10 vol.%, 7.5 vol.%, respectively) for SSPM experiments.

References

1. Tao, W. *et al.* Black Phosphorus Nanosheets as a Robust Delivery Platform for Cancer Theranostics. *Adv. Mater.* **29**, 1603276 (2017).
2. Zhang, Y.-H. *et al.* Improving gas sensing properties of graphene by introducing dopants and defects: a first-principles study. *Nanotechnology* **20**, 185504 (2009).
3. Mueller, T., Xia, F. N. A. & Avouris, P. Graphene photodetectors for high-speed optical communications. *Nat. Photonics* **4**, 297–301 (2010).
4. Song, Y. J., Qu, K. G., Zhao, C., Ren, J. S. & Qu, X. G. Graphene Oxide: Intrinsic Peroxidase Catalytic Activity and Its Application to Glucose Detection. *Adv. Mater.* **22**, 2206–2210 (2010).
5. Geim, A. K. & Novoselov, K. S. The rise of graphene. *Nat. Mater.* **6**, 183–191 (2007).
6. Wang, Q. H., Kalantar-Zadeh, K., Kis, A., Coleman, J. N. & Strano, M. S. Electronics and optoelectronics of two-dimensional transition metal dichalcogenides. *Nat. Nanotechnol.* **7**, 699–712 (2012).
7. Lu, S. B. *et al.* Third order nonlinear optical property of Bi_2Se_3 . *Opt. Express* **21**, 2072–2082 (2013).
8. Zhang, H. *et al.* Z-scan measurement of the nonlinear refractive index of graphene. *Opt. Lett.* **37**, 1856–1858 (2012).
9. Woodward, R. I. *et al.* Wideband saturable absorption in few-layer molybdenum diselenide (MoSe_2) for Q-switching Yb-, Er- and Tm-doped fiber lasers. *Opt. Express* **23**, 20051–20061 (2015).
10. Zhang, M. *et al.* Solution processed MoS_2 -PVA composite for sub-bandgap mode-locking of a wideband tunable ultrafast Er: fiber laser. *Nano Res.* **8**, 1522–1534 (2015).
11. Xia, F. N., Wang, H. & Jia, Y. C. Rediscovering black phosphorus as an anisotropic layered material for optoelectronics and electronics. *Nat. Commun.* **5**, 4458 (2014).
12. Liu, H., Du, Y. C., Deng, Y. X. & Ye, P. D. Semiconducting black phosphorus: synthesis, transport properties and electronic applications. *Chem. Soc. Rev.* **44**, 2732–2743 (2015).
13. Wang, X. M. & Lan, S. F. Optical properties of black phosphorus. *Adv. Opt. Photonics* **8**, 618–655 (2016).

14. Guo, Z. *et al.* From Black Phosphorus to Phosphorene: Basic Solvent Exfoliation, Evolution of Raman Scattering, and Applications to Ultrafast Photonics. *Adv. Funct. Mater.* **25**, 6996–7002 (2015).
15. Liu, H. *et al.* Phosphorene: An Unexplored 2D Semiconductor with a High Hole Mobility. *ACS Nano* **8**, 4033–4041 (2014).
16. Li, L. *et al.* Black phosphorus field-effect transistors. *Nat. Nanotechnol.* **9**, 372–377 (2014).
17. Buscema, M. *et al.* Fast and Broadband Photoresponse of Few-Layer Black Phosphorus Field-Effect Transistors. *Nano Lett.* **14**, 3347–3352 (2014).
18. Wang, X. M. *et al.* Highly anisotropic and robust excitons in monolayer black phosphorus. *Nat. Nanotechnol.* **10**, 517–521 (2015).
19. Suess, R. J., Jadidi, M. M., Murphy, T. E. & Mittendorff, M. Carrier dynamics and transient photobleaching in thin layers of black phosphorus. *Appl. Phys. Lett.* **107**, 081103 (2015).
20. Wang, Y. *et al.* Ultrafast recovery time and broadband saturable absorption properties of black phosphorus suspension. *Appl. Phys. Lett.* **107**, 091905 (2015).
21. Wang, K. *et al.* Ultrafast Nonlinear Excitation Dynamics of Black Phosphorus Nanosheets from Visible to Mid-Infrared. *ACS Nano* **10**, 6923–6932 (2016).
22. Nikolaenko, A. E. *et al.* Nonlinear graphene metamaterial. *Appl. Phys. Lett.* **100**, 181109 (2012).
23. Wang, Q. *et al.* Valley Carrier Dynamics in Monolayer Molybdenum Disulfide from Helicity-Resolved Ultrafast Pump-Probe Spectroscopy. *ACS Nano* **7**, 11087 (2013).
24. Lu, S. B. *et al.* Broadband nonlinear optical response in multi-layer black phosphorus: an emerging infrared and mid-infrared optical material. *Opt. Express* **23**, 11183–11194 (2015).
25. Youngblood, N., Peng, R., Nemilentsau, A., Low, T. & Li, M. Layer Tunable Third-Harmonic Generation in Multilayer Black Phosphorus. *ACS Photon.* **4**, 8–14 (2016).
26. Zheng, X. *et al.* Characterization of nonlinear properties of black phosphorus nanoplatelets with femtosecond pulsed Z-scan measurements. *Opt. Lett.* **40**, 3480–3483 (2015).
27. Chen, Y. *et al.* Mechanically exfoliated black phosphorus as a new saturable absorber for both Q-switching and Mode-locking laser operation. *Opt. Express* **23**, 12823–12833 (2015).
28. Li, D. A. *et al.* Polarization and Thickness Dependent Absorption Properties of Black Phosphorus: New Saturable Absorber for Ultrafast Pulse Generation. *Sci. Rep.* **5**, 15899 (2015).
29. Durbin, S. D., Arakelian, S. M. & Shen, Y. R. Laser-Induced Diffraction Rings from a Nematic-Liquid-Crystal Film. *Opt. Lett.* **6**, 411–413 (1981).
30. Khoo, I. C., Michael, R. R. & Yan, P. Y. Optically-Induced Molecular-Reorientation in Nematic Liquid-Crystals and Nonlinear Optical Processes in the Nanoseconds Regime. *IEEE J. Quantum Elect.* **23**, 267–272 (1987).
31. Ji, W., Chen, W. Z., Lim, S. H., Lin, J. Y. & Guo, Z. X. Gravitation-dependent, thermally-induced self-diffraction in carbon nanotube solutions. *Opt. Express* **14**, 8958–8966 (2006).
32. Wu, R. *et al.* Purely coherent nonlinear optical response in solution dispersions of graphene sheets. *Nano Lett.* **11**, 5159–5164 (2011).
33. Sadrolhosseini, A. R., Rashid, S. A., Shojanazeri, H., Noor, A. S. M. & Nezakati, H. Spatial self-phase modulation patterns in graphene oxide and graphene oxide with silver and gold nanoparticles. *Opt. Quant. Electron.* **48**, 1–13 (2016).
34. Shi, B. *et al.* Broadband ultrafast spatial self-phase modulation for topological insulator Bi₂Te₃ dispersions. *Appl. Phys. Lett.* **107**, 151101 (2015).
35. Wang, W., Wu, Y., Wu, Q., Hua, J. & Zhao, J. Coherent Nonlinear Optical Response Spatial Self-Phase Modulation in MoSe₂ Nano-Sheets. *Sci. Rep.* **6**, 22072 (2016).
36. Wang, G. *et al.* Tunable nonlinear refractive index of two-dimensional MoS₂, WS₂, and MoSe₂ nanosheet dispersions [Invited]. *Photon. Res.* **3**, A51 (2015).
37. Zhang, J. D. *et al.* Broadband spatial self-phase modulation of black phosphorus. *Opt. Lett.* **41**, 1704–1707 (2016).
38. Boyd, R. W. *Nonlinear Optics*. 210 (Academic press, 2008).
39. Qiao, J., Kong, X., Hu, Z.-X., Yang, F. & Ji, W. Few-layer black phosphorus: emerging direct band gap semiconductor with high carrier mobility. *Nat. Commun.* **5**, 4475 (2014).

Acknowledgements

This work was supported by National Natural Science Foundation of China (Grant No. 61475102) and China Scholarship Council.

Author Contributions

L.L.M., B.X.S., and C.J.Z. designed the research; L.L.M., B.X.S., and Y.Q.J. performed the experiments; J.Y. provided reagents and technical support; L.L.M., B.X.S., and C.J.Z. analyzed the data and wrote the paper. S.C.W. supervised the project. All authors reviewed the manuscript.

Additional Information

Supplementary information accompanies this paper at doi:10.1038/s41598-017-03667-z

Competing Interests: The authors declare that they have no competing interests.

Publisher's note: Springer Nature remains neutral with regard to jurisdictional claims in published maps and institutional affiliations.



Open Access This article is licensed under a Creative Commons Attribution 4.0 International License, which permits use, sharing, adaptation, distribution and reproduction in any medium or format, as long as you give appropriate credit to the original author(s) and the source, provide a link to the Creative Commons license, and indicate if changes were made. The images or other third party material in this article are included in the article's Creative Commons license, unless indicated otherwise in a credit line to the material. If material is not included in the article's Creative Commons license and your intended use is not permitted by statutory regulation or exceeds the permitted use, you will need to obtain permission directly from the copyright holder. To view a copy of this license, visit <http://creativecommons.org/licenses/by/4.0/>.

© The Author(s) 2017